Beadspring models for an adsorbed polymer molecule in a shear flow

John Atkinson, C. J. Goh, and Nhan PhanThien

Citation: The Journal of Chemical Physics **80**, 6305 (1984); doi: 10.1063/1.446700
View online: http://dx.doi.org/10.1063/1.446700
View Table of Contents: http://scitation.aip.org/content/aip/journal/jcp/80/12?ver=pdfcov
Published by the AIP Publishing

Articles you may be interested in

Development of bead-spring polymer models using the constant extension ensemble
J. Rheol. **49**, 963 (2005); 10.1122/1.2008294

Variance reduced Brownian simulation of a bead-spring chain under steady shear flow considering hydrodynamic interaction effects
J. Chem. Phys. **113**, 4767 (2000); 10.1063/1.1288803

A colloidal crystal modeled by bead–spring cubes
J. Chem. Phys. **111**, 8182 (1999); 10.1063/1.480152

Brownian dynamics simulation of bead–spring chain models for dilute polymer solutions in elongational flow
J. Rheol. **39**, 285 (1995); 10.1122/1.550722

Polymer migration phenomena based on the general beadspring model for flexible polymers
J. Chem. Phys. **80**, 5821 (1984); 10.1063/1.446608

This article is copyrighted as indicated in the article. Reuse of AIP content is subject to the terms at: http://scitation.aip.org/termsconditions. Downloaded to IP: 149.106.210.114 On: Sun, 23 Nov 2014 18:03:34

Bead-spring models for an adsorbed polymer molecule in a shear flow

John Atkinson, C. J. Goh, and Nhan Phan-Thien
Department of Mechanical Engineering, The University of Sydney, New South Wales 2006, Australia

(Received 17 August 1983; accepted 18 January 1984)

A bead-spring (Rouse-type) model is used to model an adsorbed fragment of a long-chain polymer attached to a surface in a steady shear flow. Analytic solution of the moment equations for the case of linear Hookean springs gives the mean configuration, wall traction, and power dissipation of the segment. A Monte Carlo method based on simulation of the stochastic differential equations of motion is used to deal with nonlinear finite-extension springs. The large increase in hydrodynamic thickness with shear rate found by some experimenters cannot be obtained with these models, although some increase can be obtained if there is an elongational component in the flow, due perhaps to surface nonuniformity or interference between segments.

I. INTRODUCTION

Adsorption of flexible long chain polymers at a solid liquid interface occurs in a variety of important technical situations (e.g., enhanced oil recovery, lubrication, filtration). Such an adsorbed layer affects the flow past it. Macroscopically, it is as though the wall was moved into the flow a distance L_H, the hydrodynamic thickness of the layer. Clearly, the magnitude of L_H will depend on adsorption density, on the size of a molecule (specified, e.g., by its rms radius of gyration, or its rms end-to-end distance, in free solution) and on the strength of adsorption. For so-called "weak" adsorption it is generally accepted that for each molecule one or more segments ("trains") are tightly anchored to the surface, the remaining segments ("loops" and "tails") extending into the flow. Clearly, L_H will depend on the length of these loops and tails, and on the distance to which they rise above the surface. This distance is the only variable affecting L_H which can be itself affected by the strength of the flow, at least over times short compared with that required for the degree of adsorption to change (which is of the order of days).

Experimental results[1–4] for high-molecular-weight polymers indicate that L_H can be quite large compared with the size of the molecule in free stationary solution. In particular, Gramain and Myard,[2] in experiments involving flow through commercial filters with adsorbed polyacrylamide and polystyrene over a wide range of shear rates, show that L_H increases monotonically by a factor of 3–6 as shear rate increases. This contrasts strongly with the shear thinning (decrease in viscosity with shear rate) which occurs in solutions of these molecules.

On the other hand, Cohen and Metzner,[3] using fairly concentrated (1%–4%) solutions of the same polymers in glass capillaries, obtain very large L_H which decrease by a factor of 2 as the shear rate increases. Lee and Fuller,[4] using an optical method (ellipsometry) to measure thickness of an adsorbed layer of polystyrene in flow between parallel plates, obtain a small decrease at very large shear rates. It is difficult to reconcile these various results. The experimental conditions differed widely and it seems likely that different effects were dominant in each case. This is discussed in more detail in Sec. V below.

Bead-spring models have been widely used for long-chain polymer molecules in solution.[5] Dimarzio and Rubin[6] have developed expressions for the mean configuration and power dissipation of a model of a molecule in a constant shear flow consisting of one or more beads and springs in series attached at one end to the wall ("tail" configuration). Only linear (Hookean) springs are used and an approximation is made which essentially neglects the momentum transferred to the beads by reflection from the wall, and hence leads to erroneous results for the multibead case. Fuller[7] has dealt in more detail with the single-bead model, including the loop case with two springs attached to different points, obtaining expressions for the mean dynamic response in a time-dependent shear flow. Again only linear springs are dealt with. Both authors show that the components of mean and mean-square displacement perpendicular to the wall (and hence L_H) are independent of shear rate.

In the present work time-varying flow is not considered. Exact expressions are presented for multibead linear spring segments (including the limit as the number of beads tends to infinity). In particular, the mean configuration of a segment (loop or tail), the traction it exerts on the wall and the power it dissipates are obtained. The moment-equation method used is applicable only to linear-spring models, so in order to study nonlinear models, in particular the Warner finite-extension spring, Monte Carlo simulation of the equations of motion of the segment (Langevin-type stochastic differential equations) has been used. The Warner model leads to the segment being drawn closer to the surface as shear rate increases, as might be expected. In fact, no plausible nonlinearity could cause the large increase in hydrodynamic thickness found by Gramain and Myard,[2] provided the flow remained a simple shear flow. In the last section, the effect of an elongational flow component, such as might be due to surface nonuniformities or to the flow weaving between many segments, is considered. A simplified analysis is undertaken which does lead to increasing L_H and could explain many of their experimental results.

II. THE BEAD-SPRING MODEL

A. Description of the model

The model adopted in this paper for a molecular segment consists of N identical beads connected in line to each

 0021-9606/84/126305-13$02.10 © 1984 American Institute of Physics

This article is copyrighted as indicated in the article. Reuse of AIP content is subject to the terms at: http://scitation.aip.org/termsconditions. Downloaded to IP: 149.106.210.114 On: Sun, 23 Nov 2014 18:03:34

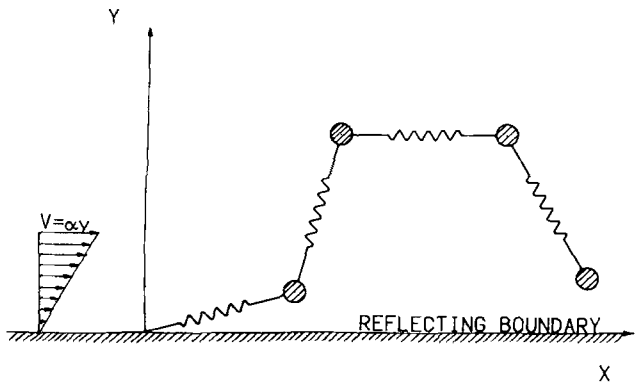

FIG. 1. Geometry of the Rouse model for a polymer molecule attached to an interface.

other and to the surface (at one end for a tail, both for a loop) by springs of zero unextended length (Fig. 1). The position of the ith bead is $\mathbf{r}_i$, the first bead is attached to the surface at $\mathbf{r}_0 = 0$, and in the case of a loop, the Nth bead is attached to

$$\mathbf{r}_{N+1} = (x_{N+1}, 0, z_{N+1});$$

it is convenient to take $\mathbf{r}_{N+1} = \mathbf{r}_N$ in the case of a tail, so that the (nonexistent) $(N+1)$th spring exerts no force. The beads are restricted to remain above the surface $y = 0$, undergoing specular reflection when they impact this surface. The fluid above the surface is Newtonian and has velocity $\mathbf{v} = \mathbf{L}\mathbf{r}$, where $\mathbf{L}$ is the velocity gradient tensor; in the case of simple shear flow, $L_{12} = \gamma$, and all other $L_{ij} = 0$.

Inertia forces due to bead mass m are known to be negligible for this type of model.[5] We also neglect hydrodynamic interaction forces between beads, both in the same loop or tail, and in neighboring segments. This assumption is less justifiable, since the polymers in the adsorbed layer are much closer together than is the case in dilute solution, where the use of bead-spring models has been most successful. In addition, we assume zero radius for the beads, but associate with each a friction coefficient β, leading to a friction force $\beta(\dot{\mathbf{r}} - \mathbf{v})$. In addition, there is a random Brownian motion force $\beta\mathbf{n}_i(t)$ acting on each load, where $\mathbf{n}(t)$ represents white noise with zero mean and correlation tensor

$$\langle \mathbf{n}_i(t)\mathbf{n}_j(t+\tau)\rangle = 2D\,\mathbf{I}\delta_{ij}\delta(\tau), \quad D = kT/\beta, \tag{2.1}$$

where kT is the Boltzmann temperature. Each spring exerts a restoring force $K(\rho)\boldsymbol{\rho}$ when its ends are separated by $\boldsymbol{\rho}$. In the case of the Rouse model with Hookean (linear) springs, K has the constant value K_0. Various nonlinear spring models have been proposed; here we use the Warner finite extension model[8] with

$$K(\rho) = K_0[1 - (\rho/R)^2]^{-1}, \tag{2.2}$$

where R is the maximum extension of each spring.

B. Scaling

By suitable choice of the units of length and time, the two parameters $\tau_1 = \beta/K_0$ (the relaxation time of a single bead spring) and $D = kT/\beta$ (the diffusivity due to Brownian force) can be taken as unity (equivalently nondimensionalize using these quantities). Then the characteristic length and time scales of each bead-spring pair will be of order unity. For simplicity this choice will be made in most of what follows. Adjustable parameters remaining in the model are bead number N and parameters such as R specifying nonlinearities.

To calibrate the model, it seems appropriate to choose spring constant K_0 and friction coefficient β to be such that a similar bead-spring model of a molecule in free solution away from a surface should behave correctly. Such an equivalent molecule is a chain with the same number N_0 of springs (i.e., $N_0 = N + 1$ for tails, $N_0 = N + 2$ for loops). As properties to be matched, we choose $\langle s^2\rangle^{1/2}$, the rms radius of gyration, and $[\eta]_0\eta_s M/\tilde{N}$, the contribution to low-shear-rate viscosity of a single molecule per unit volume. Here $[\eta]_0$ = intrinsic viscosity as $\gamma \to 0$, η_s = solvent viscosity, M = molecular weight, and $\tilde{N}$ = Avogardro's number.

For an N_0-bead molecule with Warner springs (2.2) and no hydrodynamic interaction we have, following Bird *et al.*[5] and Warner[8]

$$\langle s^2\rangle^{1/2} = \tfrac{1}{2}[(N_0^2 - 1)/N_0]^{1/2}\left(\frac{D\beta}{K_0}\right)^{1/2}(1 + 5b^{-2})^{-1}, \tag{2.3}$$

$$[\eta_0]\eta_s M/\tilde{N} = \tfrac{1}{12}(N_0^2 - 1)kT\left(\frac{\beta}{K_0}\right)(1 + 5b^{-2})^{-1}, \tag{2.4}$$

where

$$b = \left(\frac{K_0}{\beta D}\right)^{1/2} R \tag{2.5}$$

is a dimensionless measure of the maximum spring extension. For typical molecules consisting of 10^3–10^5 monomers b will take values of order 5–50. The corresponding results for the Rouse molecule, with Hookean springs, are obtained by letting $b \to \infty$. Then, in order to compare models with different parameters, or in different flows, all quantities should be rendered dimensionless using $\langle s^2\rangle^{1/2}$ as length scale and

$$\lambda = 4M[\eta_0]\eta_s/\tilde{N}kT$$

as time scale.

Note that, in terms of units with $\tau_1 = D = 1$, corresponding nonlinear molecules with different bead numbers have R varying such that

$$R^{(ND)} = R/\langle s^2\rangle^{1/2} = 2\left(\frac{N_0}{N_0^2 - 1}\right)^{1/2} R(1 + 5b^{-2}) \tag{2.6}$$

remains constant, and corresponding shear flows have γ varying such that

$$\gamma^{(ND)} = \gamma\lambda = \tfrac{1}{3}(N_0^2 - 1)\gamma(1 + 5b^{-2})^{-1} \tag{2.7}$$

remains constant.

C. The governing equations

Since the inertia term is negligible, the forces acting on the ith bead sum to zero, leading to the stochastic differential equation

$$\frac{d\mathbf{r}_i}{dt} + \beta^{-1}\{\boldsymbol{\rho}_i K(\rho_i) - \boldsymbol{\rho}_{i+1}K(\rho_{i+1})\} = \mathbf{L}\mathbf{r}_i + \mathbf{n}_i(t), \quad i = 1,2,\ldots,N, \tag{2.8}$$

This article is copyrighted as indicated in the article. Reuse of AIP content is subject to the terms at: http://scitation.aip.org/termsconditions. Downloaded to IP: 149.106.210.114 On: Sun, 23 Nov 2014 18:03:34

where $\boldsymbol{\rho}_i = \mathbf{r}_i - \mathbf{r}_{i-1}$,

$$\langle \mathbf{n}_i(t)\mathbf{n}_j(t+\tau)\rangle = 2\mathbf{I}\delta_{ij}\delta(\tau),$$

and ρ_i is the modulus of $\boldsymbol{\rho}_i$. The joint probability density function $p(\mathbf{r}_1, \mathbf{r}_2,...,\mathbf{r}_N)$ of the displacements $\mathbf{r}_i$ thus satisfies the corresponding Fokker–Planck–Kolmogorov equation, or configuration-space diffusion equation

$$\frac{\partial p}{\partial t} = \sum_{i=1}^{N} \frac{\partial}{\partial \mathbf{r}_i}\cdot\left[\frac{\partial p}{\partial \mathbf{r}_i} + \beta^{-1}\{\boldsymbol{\rho}_i K(\rho_i) - \boldsymbol{\rho}_{i+1}K(\rho_{i+1})\}p - \mathbf{L}\mathbf{r}_i\, p\right] \tag{2.9}$$

with the boundary conditions at the wall

$$\frac{\partial p}{\partial y_i} + \beta^{-1}\{(y_i - y_{i-1})K(\rho_i) - (y_{i+1} - y_i)K(\rho_{i+1})\} = 0, \quad \text{at } y_i = 0 \tag{2.10}$$

corresponding to zero flux of probability (reflection).

Of particular interest are the effects of the adsorbed molecules on wall shear stress and the power required to maintain the flow. For steady flow, the mean traction on the wall due to a single tail or loop $\mathbf{T}_w$ equals the sum of the mean friction forces on its beads, so that

$$\mathbf{T}_w = \beta\mathbf{L}\sum_{i=1}^{N}\langle \mathbf{r}_i\rangle . \tag{2.11}$$

For simple shear flow, $\mathbf{T}_w$ is parallel to the wall and has magnitude

$$T_w = \beta\gamma\sum_{i=1}^{N}\langle y_i\rangle . \tag{2.12}$$

Similarly, the mean power dissipated by a single tail or loop is

$$P_s = \beta\sum_{i=1}^{N}\langle \mathbf{r}_i^T\mathbf{L}^T\mathbf{L}\mathbf{r}_i\rangle \tag{2.13}$$

or

$$P_s = \beta\gamma^2\sum_{i=1}^{N}\langle y_i^2\rangle \tag{2.14}$$

for simple shear flow.

The hydrodynamic thickness L_H of the adsorbed polymer layer depends on the density of adsorbed segments as well as the extension of each one into the flow. Suppose there are σ identical segments each of length N per unit area. Since the flow rate with the adsorbed layer on the wall at $y = 0$ is the same as that with no layer and wall at $y = L_H$,

$$\int_o^a \langle v(y)\rangle\, dy = \int_{L_H}^a \gamma(y - L_H)\, dy, \tag{2.15}$$

where $v(y)$ is the streamwise velocity at y, and $y = a$ is well outside the adsorbed layer. But the total shear stress at y equals that at a, so

$$\sigma T(y) + \eta\frac{d}{dy}\langle v(y)\rangle = \eta\gamma , \tag{2.16}$$

where $T(y)$ is the mean horizontal force transmitted across the plane at y by one segment. Eliminating $\langle v\rangle$ from Eq. (2.15) using Eq. (2.16) gives

$$L_H = \frac{\sigma}{\gamma a\eta}\int_0^a dy\int_o^y T(y')\, dy' ,$$

but

$$T(y) = \beta\sum_{y_i>y}\left\langle y_i\frac{dv}{dy}(y_i)\right\rangle = \beta\sum_{i=1}^{N}\left\langle y_i\frac{dv}{dy}(y_i)\, U(y_i - y)\right\rangle ,$$

where U denotes the unit step function. Integrating and using $a \gg L_H$ gives

$$L_H = \frac{\beta\sigma}{\gamma\eta}\sum_{i=1}^{N}\left\langle y_i^2\frac{dv}{dy}(y_i)\right\rangle . \tag{2.17}$$

If the segments are sparse enough so that their effect on the flow is small and $dv/dy = \gamma$ to first order, then

$$L_H = \frac{\sigma\beta}{\eta}\sum_{i=1}^{N}\langle y_i^2\rangle + O\left(\frac{\sigma^2\beta^2}{\gamma^2}\langle y_i^3\rangle\right). \tag{2.18}$$

This assumption is equivalent to $L_H \ll \langle y_N^2\rangle^{1/2}$. Note that to this order L_H is proportional to the mean power dissipated by a segment. An analogous argument based on energy conservation also leads to Eq. (2.18).

Generalization of the above results to a layer consisting of a distribution of tails and loops of varying lengths is straightforward.

III. EXACT SOLUTIONS FOR THE ROUSE MODEL

A. Distribution function for y

It is apparent that the only cases which need be considered are tails attached at the origin $\mathbf{r} = 0$, and loops both of whose ends are attached to $\mathbf{r} = 0$. For if a loop were attached at two different points $\mathbf{r}_0 = (x_0,0,z_0)$ and

$$\mathbf{r}_{N+1} = (x_{N+1},0,z_{N+1}),$$

the transformation

$$\mathbf{r}_k^{(\text{new})} = \mathbf{r}_k - [(N-k+1)\mathbf{r}_0 + k\mathbf{r}_{N+1}]/(N+1) \tag{3.1}$$

moves both these points to the origin while leaving unchanged the equations of motion (2.8). This is true only for linear Hookean springs, i.e., $K(\rho)/\beta = 1$.

We treat only the steady-state case of constant flow here, although the methods used below can also be applied to the transient or harmonically forced case. The configuration-space diffusion equation (2.9) becomes

$$\sum_{i=1}^{N}\left[\frac{\partial}{\partial \mathbf{r}_i}\cdot\left\{\left(\frac{\partial}{\partial \mathbf{r}_i}\sum_{j=1}^{N}A_{ij}\,\mathbf{r}_j\right)p\right\} - \gamma y_i\frac{\partial p}{\partial x_i}\right] = 0 , \tag{3.2}$$

where the "Rouse" matrices $\mathbf{A}$ ($= \mathbf{A}^T$ for tails, $\mathbf{A}^L$ for loops) are symmetric tridiagonal matrices with

$$A_{ii} = 2, \quad A_{i,i+1} = -1 \quad \text{for } i = 1,2,...,N-1, \quad A^T_{NN} = 1, \quad A^L_{NN} = 2. \tag{3.3}$$

The inverse or "Kramers" matrices $\mathbf{B} = \mathbf{A}^{-1}$ will be required later and are given by

$$B^T_{ij} = \min(i,j), \quad B^L_{ij} = (N+1)^{-1}\min[i(N+i-j), j(N+1-i)]. \tag{3.4}$$

Integrating Eq. (3.2) over all values of the $2N$ variables x_i, z_i, and noting that the joint probability density $p \to 0$ as

This article is copyrighted as indicated in the article. Reuse of AIP content is subject to the terms at: http://scitation.aip.org/termsconditions. Downloaded to IP: 149.106.210.114 On: Sun, 23 Nov 2014 18:03:34

$|\mathbf{r}_i| \to \infty$, the following equation is obtained for the joint probability density p_y of the N variables y_i:

$$\sum_{i=1}^{N} \frac{\partial}{\partial y_i} \left\{ \left[\frac{\partial}{\partial y_i} + \sum_{j=1}^{N} A_{ij} y_j \right] p_y \right\} = 0, \tag{3.5}$$

The solution to this equation is

$$p_y = C_N \exp\left[-\frac{1}{2} \sum_{i=1}^{N+1} (y_i - y_{i-1})^2 \right], \tag{3.6}$$

where C_N is to be obtained by noting that

$$\int_0^\infty \cdots \int_0^\infty p_y \, dy,...dy_N = 1 . \tag{3.7}$$

This gives, for tails,

$$C_N = C_N^T = (2\pi)^{-1/2\,N}(2N)!!/(2N-1)!! , \tag{3.8}$$

where $n!!$ denotes $n(n-2)(n-4)...$, and for loops

$$C_N = C_N^L = (2\pi)^{-1/2\,N}(N+1)^{3/2} . \tag{3.9}$$

For proof of these formulas see the Appendix. Although we have no complete proof for $N > 3$, we believe they hold for all N, as results obtained with their use give excellent agreement with simulation up to $N = 40$.

The moment of any polynomial Q in the y_i could be obtained by integration of $Q\,p_y$. However it is more readily obtained using moment equations, as shown below. It can be seen that, as is well known for the case of a Rouse molecule in unbounded shear flow,[5] these moments are independent of shear rate. In particular, as Fuller[7] found for the single-bead case, the hydrodynamic thickness L_H of an adsorbed film is independent of shear rate, so that pressure drop along the flow direction increases linearly with flow rate.

Integrating over all x_i and y_i in Eq. (3.2), a similar equation to Eq. (3.5) is found for p_z. In this case, since the boundaries are at infinity, the z behavior of a tail is equivalent to that of an unattached Rouse molecule, while that of a loop is equivalent to an unattached ring molecule. Specifically,

$$p_z = C'_N \exp\left[-\frac{1}{2} \sum_{i=1}^{N+1} (z_i - z_{i-1})^2 \right] \tag{3.10}$$

and

$$\int_{-\infty}^{\infty} p_z \, dz = 1,$$

so that

$$C'_N = (2\pi)^{-1/2\,N} \quad \text{for tails} \tag{3.11}$$

$$= (N+1)^{1/2}(2\pi)^{-1/2\,N} \quad \text{for loops.} \tag{3.12}$$

It is readily seen that the moments involving the x_i and y_i are independent of the values of the z_i. Thus, in what follows, we need consider only the variables x_i and y_i, the problem being reduced to two dimensions. (This is true only for linear Langevin equations; in nonlinear cases, such as the finite-extension spring, there is coupling between z and the other directions.)

B. The moment equations

Let Q be any polynomial in the x_i and y_i. If the diffusion equation (3.2) is multiplied by Q and integrated over all accessible values of $\mathbf{r}_i$ ($-\infty < x_i, z_i < \infty, 0 < y_i < \infty$), the following moment equation is obtained:

$$\sum_{i,j=1}^{N} A_{ij} \left\langle r_j \frac{\partial Q}{\partial \mathbf{r}_i} \right\rangle = \sum_{i=1}^{N} \left[\left\langle \frac{\partial^2 Q}{\partial \mathbf{r}_i^2} \right\rangle + \gamma \left\langle y_i \frac{\partial Q}{\partial x_i} \right\rangle + B\left(\frac{\partial Q}{\partial y_i} \middle| y_i = 0 \right) \right] . \tag{3.13}$$

Here the terms

$$B(g|y_i = 0) = \int_{-\infty}^{\infty} d\mathbf{x} \int_{-\infty}^{\infty} d\mathbf{z} \int_0^\infty \cdots \int_0^\infty \times [gp]_{y_i = 0} \, dy_1 \cdots dy_{i-1} \, dy_{i+1} \cdots dy_N \tag{3.14}$$

are boundary terms obtained during integration by parts. Other similar terms vanish because of the boundary conditions (2.10).

If Q is of order m in the x_i and n in the y_i, it is seen that all the moments on the left-hand side of Eq. (3.13) are of the same order, while those on the right are of maximum order $m-1$ in the x_i and $n+1$ in the y_i. Thus, if the boundary terms can be evaluated, it is possible to find any moment of the x_i and y_i, provided those involving the y_i alone are known.

If

$$Q = y_1^{j_1} y_2^{j_2} \cdots y_N^{j_N} , \tag{3.15}$$

the moment equation becomes

$$\sum_{i,j=1}^{N} A_{ij} \left\langle y_j \frac{\partial Q}{\partial y_i} \right\rangle = \sum_{i=1}^{N} \left[\left\langle \frac{\partial^2 Q}{\partial y_i^2} \right\rangle + j_i B(y_i^{-1} Q | y_i = 0) \right] , \tag{3.16}$$

where

$$B(y_i^{-1} Q | y_i = 0) = \delta_{j_1 1} \, C_N (C^L_{i-1} C_{N-i})^{-1} \times \langle y_1^{j_1} \cdots y_{i-1}^{j_{i-1}} \rangle^L_{i-1} \times \langle y_1^{j_{i+1}} \cdots y_{N-i}^{j_N} \rangle_{N-i} . \tag{3.17}$$

Here $\langle \cdot \rangle_k$ denotes the moment for the k-bead case. The superscript L on C and $\langle \cdot \rangle$ denotes the value corresponding to a loop. Absence of a superscript denotes "loop" or "tail" according to the case being considered; i.e., whether the Nth bead is attached or free. Starting from the one-bead case, Eqs. (3.16) and (3.17) enable the moments of the y_i to be evaluated for all N.

C. Mean bead displacements

If Q is set equal to y_i in Eqs. (3.16) and (3.17), then $\langle y_j \partial Q / \partial y_i \rangle = \langle y_j \rangle$, so that the simultaneous equations (3.16) solve to give

$$\langle y_i \rangle_N = C_N \sum_{j=1}^{N} B_{ij} (C^L_{j-1} C_{N-j})^{-1}, \quad i = 1,2,...,N, \tag{3.18}$$

where the B_{ij} are given by Eq. (3.4). If Q is set equal to x_i in (3.13), the boundary terms are zero, and so

$$\langle x_i \rangle_N = \gamma \sum_{j=1}^{N} B_{ij} \langle y_j \rangle_N, \quad i = 1,2...,N . \tag{3.19}$$

The symmetry of a loop about its centerpoint, together with the relation

$$B_{ij} + B_{i(N+1-j)} = 1 ,$$

This article is copyrighted as indicated in the article. Reuse of AIP content is subject to the terms at: http://scitation.aip.org/termsconditions. Downloaded to IP: 149.106.210.114 On: Sun, 23 Nov 2014 18:03:34

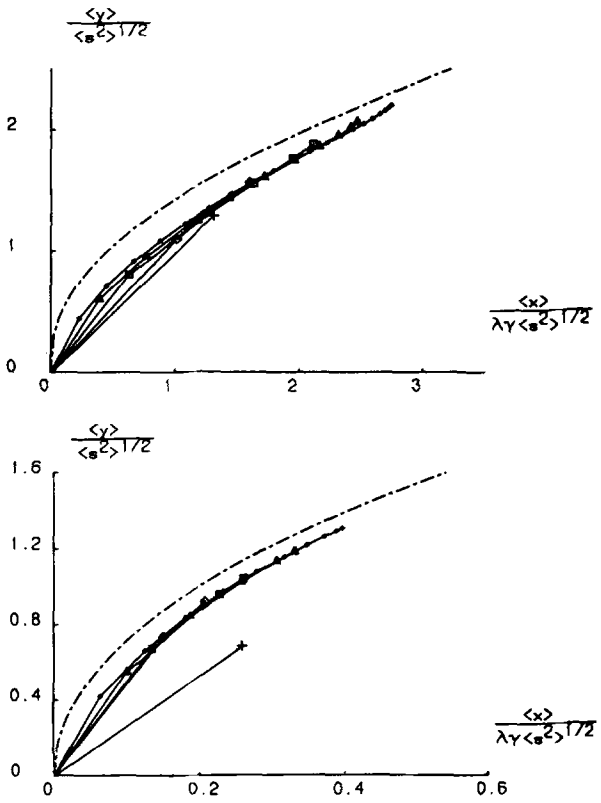

FIG. 2. (a) The mean configuration $\langle y\rangle/\langle s^2\rangle^{1/2}$ vs $\langle x\rangle/\lambda\gamma\langle s^2\rangle^{1/2}$ for the linear Rouse model for the tail case (simulations up to $N=40$ agree excellently with theory): $+$ $N=1$; ◇ $N=2$; ◆ $N=20$; □ $N=5$; --- $N=\infty$; △ $N=10$. (b) The same as Fig. 2(a), but for the loop case.

leads to the simplification

$$\langle y_i\rangle_N^L = \langle y_{N-i}\rangle^L = C_N^L \sum_{j=1}^{N/2} \min(i,j)(C_{j-1}^L\, C_{N-j}^L)^{-1},$$

$$i = 1,2,\ldots,N/2,\ N \text{ even} \tag{3.20}$$

$$= C_N^L \left[\sum_{j=1}^{(N-1)/2} \min(i,j)(C_{j-1}^L\, C_{N-j}^L)^{-1} + \frac{1}{2} i (C_{(N-1)/2}^L)^{-2}\right],$$

$$i = 1,2,\ldots,(N+1)/2,\ N \text{ odd} \tag{3.21}$$

with corresponding formulas for the $\langle x_i\rangle_N^L$.

In Fig. 2, the mean configurations for tails and loops are shown for a variety of values of N.

In order to find second order moments involving the x_i, it is necessary to find boundary terms of the form $B(x_i \mid y_j = 0)$, as defined by Eq. (3.14). For the case of a single bead, one obtains, on multiplying the diffusion equation (3.2) by x and integrating over $-\infty < x < \infty$,

$$\frac{d^2B}{dy^2} + y\frac{dB}{dy} = -\gamma y p_y(y), \tag{3.22}$$

where

$$B = \int_{-\infty}^{\infty} x p(x,y)\,dx, \quad p_y(y) = C_1 e^{-1/2y^2}. \tag{3.23}$$

The solution is $B = \frac{1}{2}\gamma \operatorname{erfc} y$, so that $B(x \mid y = 0) = \frac{1}{2}\gamma$. The moment equations (3.13) with $Q = xy$ and $Q = x^2$ then give, successively,

$$\langle xy\rangle = \tfrac{3}{2}\gamma, \quad \langle x^2\rangle = 1 + \tfrac{3}{4}\gamma^2, \tag{3.24}$$

which agree with the results in Fuller.[7] Analytic formulas have not been obtained for the corresponding moments $\langle x_i\, y_j\rangle$ and $\langle x_i\, x_j\rangle$ in the multibead case.

D. Wall traction and power dissipation

According to Eq. (2.12), the mean traction on the wall due to a single molecule is

$$T_w = \beta\gamma \sum_{i=1}^{N} \langle y_i\rangle = C_N \sum_{i,j=1}^{N} B_{ij}\,(C_{j-1}^L\, C_{N-j})^{-1}. \tag{3.25}$$

Similarly, from Eq. (2.13), the power dissipated per molecule is

$$P_s = \beta\gamma^2 \sum_{i=1}^{N} \langle y_i^2\rangle. \tag{3.26}$$

If Q in Eq. (3.13) is set equal to $\frac{1}{2}\sum B_{jk}\, y_j\, y_k$, then the left-hand side of this equation reduces to $\sum \langle y_i^2\rangle$, so that

$$P_s = \beta\gamma^2 \left[\sum_{i=1}^{N} B_{ii} + C_N \sum_{i=1}^{N} (C_{i-1}^L\, C_{N-i})^{-1} \times\left(\sum_{j=1}^{i-1} B_{ij}\langle y_j\rangle_{i-1}^L + \sum_{j=i+1}^{N} B_{ij}\langle y_j\rangle_{N-i}\right)\right]. \tag{3.27}$$

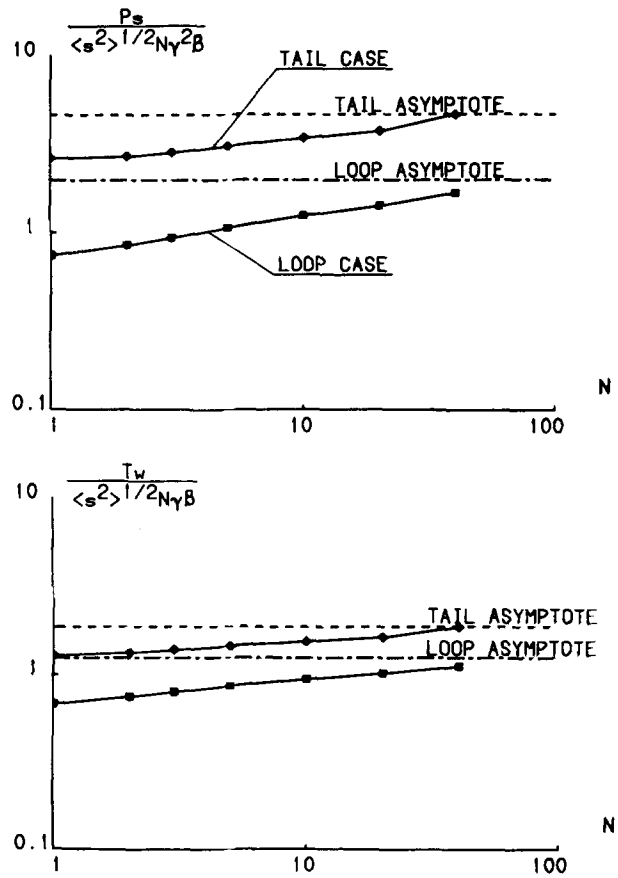

FIG. 3. (a) Power dissipation for the linear Rouse model [$(P_s/\langle s^2\rangle N\gamma^2\beta$ vs N]. (Simulations up to $N=40$ agree excellently with theory.) (b) Wall traction for the linear Rouse model [$(T_w/\langle s^2\rangle^{1/2}N\gamma\beta)$ vs N]. (Simulations up to $N=40$ agree excellently with theory.)

This article is copyrighted as indicated in the article. Reuse of AIP content is subject to the terms at: http://scitation.aip.org/termsconditions. Downloaded to IP: 149.106.210.114 On: Sun, 23 Nov 2014 18:03:34

Note that $\sum_{i=1}^{N} B_{ii}$, the trace of matrix $\mathbf{B}$, is equal to $\frac{1}{2}N(N+1)$ for tails, and $\frac{1}{6}N(N+2)$ for loops. The expression obtained by Dimarzio and Rubin[6] for P_s includes only this term, since they neglect terms due to reflection from the boundary. As N increases, however, the boundary terms become dominant (see Fig. 3).

E. Limits for large N

By letting $N\to\infty$ in the equations of the previous sections, asymptotic formulas are obtained for the mean bead displacements, wall traction, and power dissipation. Stirling's asymptotic formula for the factorial function, applied to Eq. (3.8) yields

$$C_N^T \sim (2\pi)^{-1/2} N \pi^{1/2} N^{1/2} \quad \text{as } N\to\infty\ . \tag{3.28}$$

Then if only the highest order terms in N are retained and the sums are replaced by integrals, Eq. (3.18) becomes

$$\langle y_i \rangle_N^T \sim (2\pi)^{-1/2} N^{1/2} [\cos^{-1}(1-2\alpha) + 2\alpha^{1/2}(1-\alpha)^{1/2}]\ , \tag{3.29}$$

$$\langle y_i \rangle_N^L \sim (2\pi)^{-1/2} N^{1/2} 4\alpha^{1/2}(1-\alpha)^{1/2}\ , \tag{3.30}$$

where $\alpha = i/N$. Then Eq. (3.19) gives

$$\begin{aligned}\langle x_i \rangle_N^T \sim{}& (2\pi)^{-1/2} N^{5/2}\gamma \\ &\times [\tfrac{3}{4}\pi\alpha - (\tfrac{1}{16} - \tfrac{1}{4}\alpha + \tfrac{1}{2}\alpha^2)\cos^{-1}(1-2\alpha) \\ &+ (\tfrac{1}{8} - \tfrac{5}{12}\alpha - \tfrac{1}{3}\alpha^2)\alpha^{1/2}(1-\alpha)^{1/2}]\ ,\end{aligned} \tag{3.31}$$

$$\begin{aligned}\langle x_i \rangle_N^L \sim{}& (2\pi)^{-1/2} N^{5/2}\gamma \\ &\times [\tfrac{1}{4}\pi\alpha + (\tfrac{1}{4} - \tfrac{1}{2}\alpha)\cos^{-1}(1-2\alpha) \\ &- (\tfrac{1}{2} - \tfrac{7}{3}\alpha + \tfrac{2}{3}\alpha^2)\alpha^{1/2}(1-\alpha)^{1/2}]\ .\end{aligned} \tag{3.32}$$

These results are also presented in Fig. 2. Similarly, the mean wall traction is, from Eq. (3.25),

$$T_w^T \sim \tfrac{3}{4}\left(\frac{\pi}{2}\right)^{1/2} N^{3/2}\beta\gamma, \quad T_w^L \sim \frac{1}{2}\left(\frac{\pi}{2}\right)^{1/2} N^{3/2}\beta\gamma \tag{3.33}$$

and the power dissipated by the molecule is, from Eq. (3.27)

$$P_s^T \sim \tfrac{7}{6}\beta\gamma^2 N^2, \quad P_s^L \sim \tfrac{1}{2}\beta\gamma^2 N^2\ . \tag{3.34}$$

IV. SIMULATION

A. The Monte Carlo method

The analytical methods discussed above lead to useful results for N-bead molecular segments with linear Hookean springs, including the limit as $N\to\infty$. For nonlinear models, such as that with Warner finite-extension springs, the moment-equation method does not lead to a closed set of equations, and few exact results are possible, except in the no-flow case ($\gamma = 0$). Perturbation solutions can be obtained when the nonlinearity is small (maximum extension $R \gg 1$), or when the flow is weak ($\gamma \ll \lambda_0^{-1}$). While these give a qualitative indication of the effects of nonlinearities, the results are quantitatively poor away from the linear or small-shear regime. Numerical methods are necessary to gain insight into these cases.

The technique used is a Monte Carlo type simulation similar to that of Ermak and Buckholz,[9] where the equation motion (2.8) is used to obtain a marching scheme for the state variables $\mathbf{r}_i$. Consider the general set of stochastic differential equations

$$\dot{\mathbf{r}} = \mathbf{K}\mathbf{r} + \mathbf{n}(t), \tag{4.1}$$

where matrix $\mathbf{K}$ is a function of $\mathbf{r}$. Over a sufficiently short time interval Δt, $\mathbf{K}$ is approximately constant and direct integration of Eq. (4.1) from t to $t+\Delta t$ gives

$$\begin{aligned}\mathbf{r}(t+\Delta t) = e^{-\mathbf{K}\Delta t}\mathbf{r}(t) + \int_t^{t+\Delta t} \\ \times \exp[-\mathbf{K}(t+\Delta t - t')]\,\mathbf{n}(t')\,dt'\ .\end{aligned} \tag{4.2}$$

For sufficiently small Δt, we can approximate Eq. (4.2) by

$$\mathbf{r}(t+\Delta t) = \left[\mathbf{I} - \mathbf{K}\Delta t + \frac{\mathbf{K}^2\Delta t^2}{2}\right]\mathbf{r}(t) + \mathbf{B}(t,\Delta t) + O(\Delta t^3), \tag{4.3}$$

where

$$\mathbf{B}(t,\Delta t) = e^{-\mathbf{K}(t+\Delta t)} \int_t^{t+\Delta t} e^{\mathbf{K}t'}\mathbf{n}(t')\,dt'\ . \tag{4.4}$$

Since $\mathbf{B}$ is a linear functional of the Gaussian process $\mathbf{n}(t)$, it is also Gaussian with mean

$$\langle \mathbf{B}(t,\Delta t)\rangle = \mathbf{O}$$

and covariance matrix

$$\begin{aligned}\mathbf{V}(t,\Delta t) &= \langle \mathbf{B}(t,\Delta t)\,\mathbf{B}(t,\Delta t)\rangle \\ &= \int_t^{t+\Delta t}\int_t^{t+\Delta t} \exp[-\mathbf{K}(t+\Delta t - t')]\langle \mathbf{n}(t')\,\mathbf{n}(t'')\rangle \exp[-\mathbf{K}^T(t+\Delta t - t'')]\,dt'\,dt'' \\ &= 2D\Delta t\left\{e^{-\mathbf{K}\Delta t}e^{-\mathbf{K}^T\Delta t} + \frac{\Delta t}{2}(\mathbf{K}e^{-\mathbf{K}\Delta t}e^{-\mathbf{K}^T\Delta t} + e^{-\mathbf{K}\Delta t}e^{-\mathbf{K}^T\Delta t}\mathbf{K}^T)\right\} + O(\Delta t^3)\ .\end{aligned} \tag{4.5}$$

Thus the covariance of $\mathbf{B}$ is independent of t as expected intuitively. For small Δt, Eq. (4.5) can be approximated by

$$\mathbf{V}(\Delta t) = 2D\{\Delta t\,\mathbf{I} - \tfrac{1}{2}(\mathbf{K} + \mathbf{K}^T)\Delta t^2 + O(\Delta t^3)\}\ . \tag{4.6}$$

Though Eqs. (4.3) and (4.6) are accurate to $O(\Delta t^3)$, the $O(\Delta t^2)$ terms are usually not readily available. [In particular, the second term in Eq. (4.6) represents a correlated noise which has to be generated by a reverse Gram–Schmidt process.] Computationwise, it appears to be both faster and more accurate to use only the first order correction with smaller time step, rather than to use the second order correction with larger time step.

This article is copyrighted as indicated in the article. Reuse of AIP content is subject to the terms at: http://scitation.aip.org/termsconditions. Downloaded to IP: 149.106.210.114 On: Sun, 23 Nov 2014 18:03:34

The matrix **K** has remained arbitrary so far; in the case of simple shear flow with linear springs, the instantaneous position of each bead is marched in time according to the following stochastic difference equations:

$$x_j(t+\Delta t) = (1-2\Delta t)\,x_j(t) + \Delta t x_{j-1}(t) + \Delta t x_{j+1}(t) + \gamma \Delta t y_j(t) + b_{xj}(t), \tag{4.7}$$

$$y_j(t+\Delta t) = (1-2\Delta t)\,y_j(t) + \Delta t y_{j-1}(t) + \Delta t y_{j+1}(t) + b_{yj}(t), \tag{4.8}$$

where the $b_{xj}(t)$, $b_{yj}(t)$, $j = 1,2,\ldots,N$ are uncorrelated random numbers normally distributed with zero mean and variance $2\Delta t$. As discussed in Sec. II B, appropriate scaling has been achieved by choosing units for length and time so that $D = kT/\beta$ and $\tau_1 = K_0/\beta$ are unity. Since the first spring is attached to the surface at the origin, $x_0(t) \equiv y_0(t) \equiv 0$. The lack of a second spring attached to the final bead in the tail case is obtained by setting $x_{N+1}(t) \equiv x_N(t)$ and $y_{N+1}(t) \equiv y_N(t)$. Since the final spring in the loop case is attached to the surface, here $x_{N+1}(t)$ takes a specified constant value while $y_{N+1}(t)$ is identically zero.

The reflecting boundary at $y = 0$ requires that y_j be replaced by $-y_j$ whenever y_j takes on negative values. An additional set of equations for the z_j can also be included, but is independent of those for the x_j and y_j.

The fact that the process is ergodic enables us to compute the ensemble averages of the statistical properties in terms of time averages. Thus if $G(\mathbf{r}(t))$ is any function of $\mathbf{r}(t)$, the ensemble average of $G(\mathbf{r}(t))$ is approximated by

$$\langle G(\mathbf{r}(t))\rangle = \frac{1}{T}\int_0^T G(\mathbf{r}(t))\,dt, \quad T \text{ large}. \tag{4.9}$$

Typically the time taken to reach stationarity is small compared to the time required to achieve a reasonable steady average. The required averaging time T increases approximately as N^2, as would be expected since the time scale in our units is $O(N^2)$ the physical time scale. For large N, a huge amount of computer time is thus inevitable.

B. Treatment of nonlinear Warner spring models

When using the previous scheme for nonlinear Warner spring models one has to be extremely careful about the choice of time step because of the presence of singularity when the springs reach their full extension. Due to the randomness of the noise, it is quite possible (especially when the time step is too large) that an interbead distance may exceed its maximum length R and consequently negative spring force will drive the system unstable. Another more subtle source of instability arises from the fact that the marching scheme only converges to the correct solution when the interbead distance $\rho_j(t)$ lies within a range smaller than R and dictated by Δt. Otherwise instability similar (though not quite the same) to that of homoclinic and heteroclinic oscillation may arise. These oscillations are commonly encountered in the solution of nonlinear difference equations (see, e.g., Reinhall).[10] These difficulties can be overcome by systematically halving the time step whenever any ρ_j gets too close to its singular value.

The marching scheme for the Warner model is as follows:

$$\mathbf{r}_j(t+\Delta t) = [1 - K(\rho_j(t))\Delta t - K(\rho_{j+1}(t))\Delta t] \times \mathbf{r}_j(t) + K(\rho_j)\Delta t \mathbf{r}_{j-1}(t) + K(\rho_{j+1})\Delta t \mathbf{r}_{j+1} + \gamma \Delta t y_j(t)\boldsymbol{\delta}_1 + \mathbf{b}_j(t), \tag{4.10}$$

where $K(\rho)$ is given by Eq. (2.2) and $\boldsymbol{\delta}_1$ is the unit vector (1,0,0). Displacements in all three dimensions are coupled through

$$\rho_j = [(x_j - x_{j-1})^2 + (y_j - y_{j-1})^2 + (z_j - z_{j-1})^2]^{1/2}, \tag{4.11}$$

so that it is strictly speaking not possible to disregard the equations for the z_j. Uncoupling may be achieved by using the (physically unrealistic) "two-dimensional model" with

$$\rho_j = [(x_j - x_{j-1})^2 + (y_j - y_{j-1})^2]^{1/2}. \tag{4.12}$$

End conditions ($j = 0$ and $N+1$) are the same as in the linear spring case.

If the nonlinearity is large, i.e., dimensionless maximum extension b is small, the governing scales of the problem become D and R, rather than D and τ_1 as in the linear case. The corresponding time scale is $R^2 D$. In units such that D and R are constant, the time scale is $O(N^2)$ (as in the linear case) in physical units for all b, but reduced time steps are necessary when any spring is near full extension which increases the computer time required considerably for large N, compared with the linear case.

C. Results

For segments with Hookean springs, tail and loop cases were run with bead number N up to 40. Agreement with the theoretical results exemplified in Figs. 2 and 3 was excellent, despite the approximations of the simulation method. Most results were obtained for a time step Δt of 0.1; for this value it is estimated that the discretization error obtained was less than 2% in the $\langle \mathbf{r}_i \rangle$.

For segments with nonlinear Warner springs, comparable accuracy required initial time steps considerably smaller than for linear springs (typically $\Delta t = 0.05N^{-1/2}$ for $b = \sqrt{5}$) together with a mechanism to reduce the time step whenever any ρ_j approached its maximum value too closely. Averaging time needed to eliminate statistical fluctuations [T in Eq. (4.9)] was somewhat longer than in the linear-spring case. Thus the computer time required per run was substantially larger, and in order to reduce it somewhat most runs dealt with the two-dimensional model described above, with no z_j equations.

In order to compare the simulated results with theoretical analysis, we first examine the simplest case of a single bead and these are shown in Fig. 4(a). The zero shear rate steady configuration agrees well with theoretical prediction, namely

$$\langle y\rangle = \tfrac{1}{2}\pi^{-1/2} b\,(2+b^2)\Gamma[\tfrac{1}{2}(2+b^2)]/\Gamma[\tfrac{1}{2}(5+b^2)], \tag{4.13}$$

$$\langle x^2\rangle = \langle y^2\rangle = b^2(4+b^2)^{-1}, \quad \langle x\rangle = \langle xy\rangle = 0.$$

As γ increases, the average extension of the spring increases and the locus traced out by the bead's steady state mean position for various γ appears to intersect the $\langle x\rangle$ axis at

This article is copyrighted as indicated in the article. Reuse of AIP content is subject to the terms at: http://scitation.aip.org/termsconditions. Downloaded to IP: 149.106.210.114 On: Sun, 23 Nov 2014 18:03:34

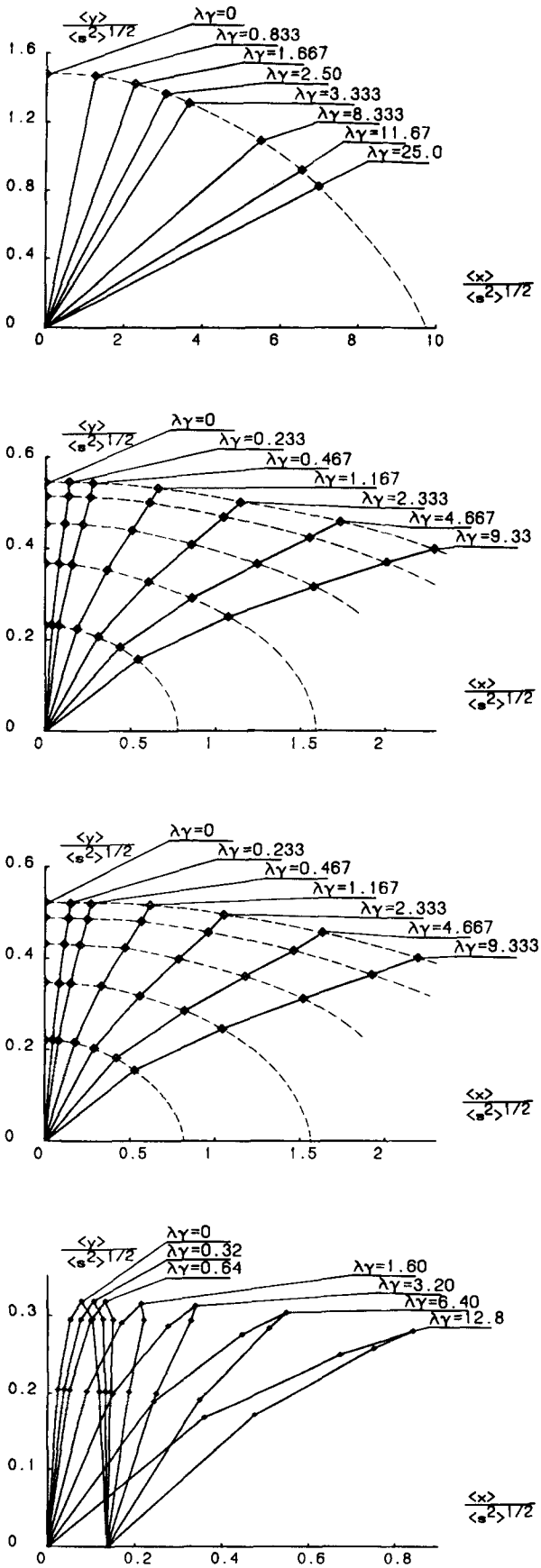

FIG. 4. (a) Effects of increasing shear rate for the nonlinear Rouse model, $b = 5$ [$(\langle y\rangle/\langle s^2\rangle^{1/2})$ vs $(\langle x\rangle/\langle s^2\rangle^{1/2})$] $N = 1$, two-dimensional tail. (b) The same as Fig. 4(a) but for $N = 5$, two-dimensional tail, $b = \sqrt{5}$. (c) The same as Fig. 4(a) but for $N = 5$, three-dimensional tail, $b = \sqrt{5}$. (d) The same as Fig. 4(a) but for $N = 5$, two-dimensional loop, $b = \sqrt{5}$.

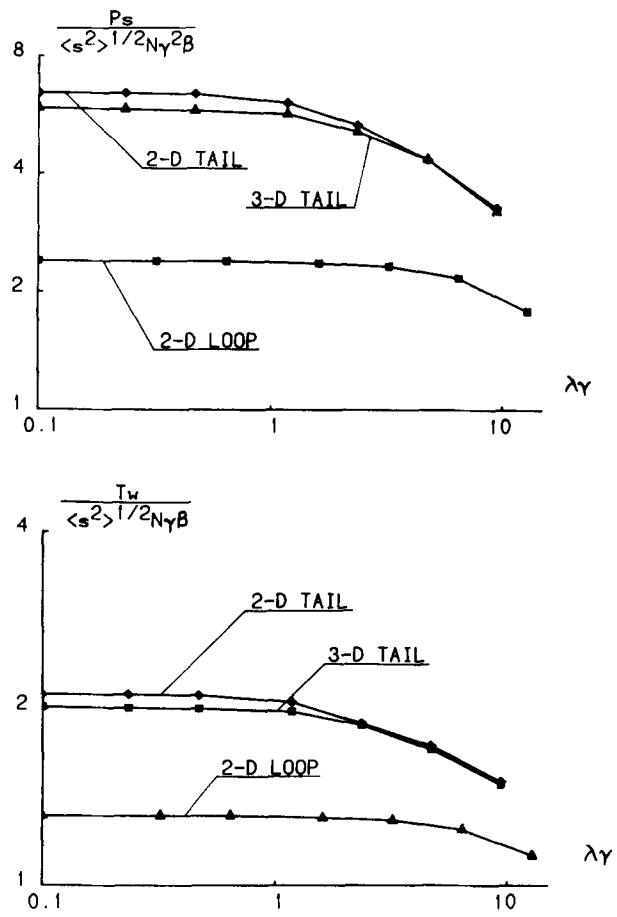

FIG. 5. (a) Power dissipation for the nonlinear Rouse model $b = \sqrt{5}$, $N = 5$ [$(P_s/\langle s^2\rangle N\gamma^2\beta)$ vs $\lambda\gamma$] for the $2D$ tail, $3D$ tail, and $2D$ loop. (b) Wall traction for the nonlinear Rouse model $b = \sqrt{5}$, $N = 5$ [$(T_w/\langle s^2\rangle^{1/2}N\gamma\beta)$ vs $\lambda\gamma$] for the $2D$ tail, $3D$ tail, and $2D$ loop.

$\langle x\rangle = b$ as $\gamma\to\infty$, as follows trivially from the equations of motion. The effect of increasing γ for $N = 5$ is computed for the case of $2D$ tail [Fig. 4(b)], $3D$ tail [Fig. 4(c)] and $2D$ loop [Fig. 4(d)] with their corresponding power dissipation and wall traction shown in Fig. 5.

Figure 5(a) illustrates a drop in power dissipation P_s/γ^2 as shear rate increases which is similar to the drop in viscosity observed by Warner.[8] In contrast, there was no sign of any change in P_s/γ^2 when linear springs were used since the moments in y are independent of γ. Various loop cases are also computed for $N = 10$ with fixed shear rate (Fig. 6). In the nonlinear-spring loop case, the results for the two ends at different points cannot be deduced trivially from those with both ends at the same point, as in the linear-spring case [Eq. (3.1)]. However, the simulation results show that the relative position of the two ends has little effect on the moments of the y_j except in extreme cases [compare Fig. 6(a) with Fig. 6(b), and Fig. 6(c) with Fig. 6(d)]. Hence it is reasonable to assume the same power dissipation characteristics for all loop cases. The simulation is also extended to the physically more realistic three-dimensional case, where excursions in the z direction reduce the maximum spring extension in the $x-y$ plane, since there is coupling between the x_i, y_i, z_i equations, although the shear flow remains strictly in the $x-y$ plane. Comparison between the two- and three-dimen-

This article is copyrighted as indicated in the article. Reuse of AIP content is subject to the terms at: http://scitation.aip.org/termsconditions. Downloaded to IP: 149.106.210.114 On: Sun, 23 Nov 2014 18:03:34

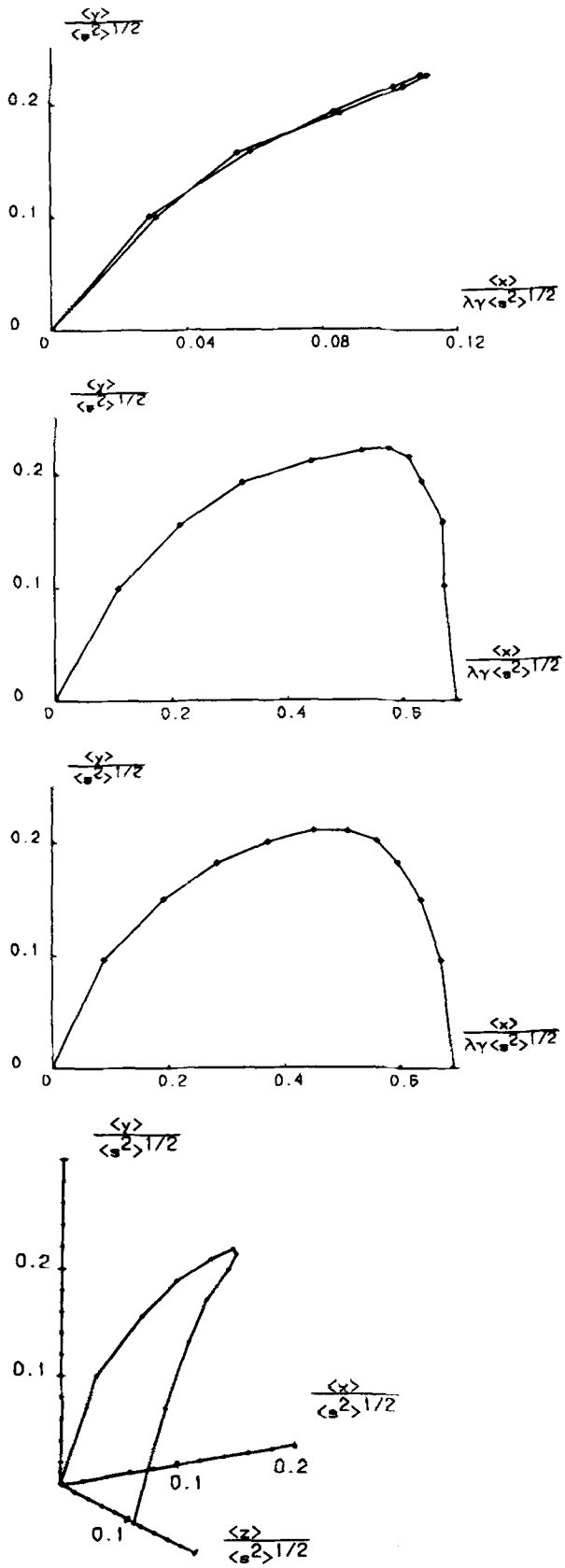

FIG. 6. (a) $2D$ loop with nonlinear Warner spring and free end tied to the origin. $N = 10$, $\lambda\gamma = 0.1589$, $b = \sqrt{5/2}$ [$(\langle y\rangle/\langle s^2\rangle^{1/2})$ vs $(\langle x\rangle/\lambda\gamma\langle s^2\rangle^{1/2})$]. (b) $2D$ loop with nonlinear Warner spring and free end tied to (0.692, 0). $N = 10$, $\lambda\gamma = 0.1589$, $b = \sqrt{5/2}$ [$(\langle y\rangle/\langle s^2\rangle^{1/2})$ vs $(\langle x\rangle/\lambda\gamma\langle s^2\rangle^{1/2})$]. (c) $3D$ loop with nonlinear Warner spring and free end tied to (0.692, 0, 0). $N = 10$, $\lambda\gamma = 0.1589$, $b = \sqrt{5/2}$ [$(\langle y\rangle/\langle s^2\rangle^{1/2})$ vs $(\langle x\rangle/\lambda\gamma\langle s^2\rangle^{1/2}$]. (d) $3D$ loop with nonlinear Warner spring and free end tied to (0, 0, 0.1099). $N = 10$, $\lambda\gamma = 0.1589$, $b = \sqrt{5/2}$ [$(\langle y\rangle/\langle s^2\rangle^{1/2}$ vs $(\langle x\rangle/\lambda\gamma\langle s^2\rangle^{1/2}$].

sional cases can be made through Fig. 4(b) with Fig. 4(c) and Fig. 6(b) and Fig. 6(c). Their results differ by only a small amount, which justifies our use of the two-dimensional model approximation in other cases.

V. COMPARISON WITH EXPERIMENTAL DATA

A. Hydrodynamic thickness at low shear rate

The Rouse (linear spring) model for a molecular segment, analyzed in Sec. III above, leads to a mean displacement from the wall somewhat larger than the radius of gyration of a free molecule of the same length (Fig. 2), due to the momentum away from the wall which is transmitted to beads when they are reflected and this effect increases to a limiting value with N the number of beads. However, the segments (loops and tails) under consideration are only a fraction of the complete molecule. Thus, one might expect a hydrodynamic thickness L_H somewhat less than the size of a complete free molecule.

The experimental results[1–4] are summarized in Table I. Here, n is the number of monomer units, R_M is the maximum extended length (based on 2.52 Å per monomer), and $\langle s^2\rangle^{1/2}$ is the radius of gyration (quoted by the experimenters in Ref. 2, estimated by us for the others). Values are given for L_H at small and large shear rates [$L_H(0)$ and $L_H(\infty)$, respectively], and for the critical shear rate γ_{cr} which is the value at which L_H equals the geometric mean of $L_H(0)$ and $L_H(\infty)$. The polymers used were hydrolyzed polyacrylamide (HPAM) in aqueous solution, and polystyrene (PS) dissolved in toluene (T), decalin (D), and cyclohexane (C).

Gramain and Myard[2] find L_H about equal to free molecular diameter for small shear rates through Millipore and Sartorius filters, with $L_H/\langle s^2\rangle^{1/2} = 1.2 - 2.5$. Lee and Fuller,[4] using ellipsometry, find a film thickness of $0.9\langle s^2\rangle^{1/2}$. Silberberg,[1] at an unquoted but presumably small shear rate, gets $L_H/\langle s^2\rangle^{1/2} = 2.5$. All these authors used a flow of solvent past a layer which had previously been deposited from a dilute solution. Their L_H values are close to the upper limit of what our model predicts, possible only if most molecules are attached at only one or two points, and if they are sufficiently closely packed that there is little or no flow between them. For Nucleopore filters, Gramain and Myard[2] obtain a much lower $L_H(0)/\langle s^2\rangle^{1/2}$, presumably corresponding to more (~ 10) points of attachment per molecule.

Cohen and Metzner[3] use fairly concentrated solutions (1% – 4%), and obtain L_H an order of magnitude larger. As Lee and Fuller[4] suggest, this can only be explained if there are multiple polymer layers present, which is outside the scope of the present model.

B. Variation with shear rate

The Rouse (linear spring) model, predicts no change in hydrodynamic thickness L_H with shear rate, so long as the flow remains strictly parallel to the wall. Our Warner (finite extension spring) model predicts a drop in L_H, becoming significant when the shear rate reaches a critical value γ_{cr}, where the horizontal extension is of the same order as the maximum extension. For a segment of maximum extension

This article is copyrighted as indicated in the article. Reuse of AIP content is subject to the terms at: http://scitation.aip.org/termsconditions. Downloaded to IP: 149.106.210.114 On: Sun, 23 Nov 2014 18:03:34

TABLE I. Experimental results from Refs. 1–4.

Polymer	$M_w \times 10^{-6}$	n	R_M μm	$\langle s^2\rangle^{1/2}$ μm	$L_H(0)$ μm	$L_H(\infty)$ μm	γ_{cr} s^{-1}	$L_H(0)/\langle s^2\rangle^{1/2}$	$R_M/L_H(\infty)$	$L_H(\infty)/L_H(0)$
PS–T[a]	1.8	17 000	4.3	0.06	0.15	...	...	2.5	...	...
HPAM 0%[b,c]	8.2	115 000	29.1	0.20	0.51	>1	500	2.55	<30	>2
	2.9	41 000	10.3	0.103	0.25	$\gtrsim 1.6$	450	2.43	$\gtrsim 6.4$	$\gtrsim 6.4$
	0.92	13 000	3.25	0.049	0.095	0.35	400	1.94	9.2	3.7
	0.32	4 500	1.13	0.020	0.045	0.18	300	2.25	6.3	4
HPAM 0%[b,d]	8.2	115 000	29.1	0.20	0.048	0.42	5000	0.24	69	8.75
HPAM 15%[b,c]	2.2	31 000	7.8	0.120	<0.6	0.9	~ 500	<5	8.7	>1.5
HPAM 35%[b,c]	2.1	29 000	7.4	0.173	<0.9	1.1	~ 500	<5	6.8	>1.2
PS–T[b,c]	8.2	79 000	19.8	0.20	~ 0.35	$\gtrsim 0.6$	~ 800	~ 1.75	$\lesssim 33$	$\gtrsim 1.7$
	2.4	23 000	5.8	0.098	~ 0.12	$\gtrsim 0.25$	~ 1600	~ 1.22	$\lesssim 23$	$\gtrsim 2.1$
HPAM[e]	1.75	24 500	6.2	0.10	$\gtrsim 1.5$	$\lesssim 0.8$	$\lesssim 600$	$\gtrsim 15$	$\gtrsim 8$	$\lesssim 0.5$
PS–T[e]	1.8	17 000	4.3	0.06	$\gtrsim 1.5$	0.8	$\lesssim 200$	$\gtrsim 25$	5.4	$\lesssim 0.5$
PS–D[e]	1.5	17 000	4.3	0.06	$\gtrsim 1.5$	0.9	$\lesssim 500$	$\gtrsim 25$	4.8	$\lesssim 0.6$
PS–C[f]	20	190 000	48	0.3	0.26	<0.23	>6000	0.9	>210	<0.9

[a] FromFig. 2 of Silberberg (Ref. 1); glass capillaries, radius 257 μm; shear rate not quoted.
[b] From Table II and Figs. 1–6 of Gramain and Myard; 0% etc. represent degrees of hydrolysis.
[c] Various Millipore and Sartorius filters, mean radius 1.5–1.6 μm.
[d] Nuclepore filters, mean radius 2.25 μm.
[e] From Cohen and Metzner (Ref. 3); concentrated solutions in glass capillaries, radius 90–260 μm.
[f] From Lee and Fuller (Ref. 4); parallel plates 0.6 mm apart with adsorbed thickness "L_H" measured by ellipsometry.

R and radius of gyration $\langle s^2\rangle^{1/2}$,

$$\gamma_{cr} = c\lambda^{-1} R/\langle s^2\rangle^{1/2},$$

where

$$\lambda = 4M[\eta_0]\eta_s/\tilde{N}kT$$

is the time scale defined in Sec. II B and the constant c is about 1.5 for a tail and 0.25 for a loop [obtained by setting $\langle x_n\rangle \simeq \frac{1}{2} R$ in Eqs. (3.31) and (3.32), or from the Warner molecule simulation of Fig. 4]. Using values for $\langle\eta_0\rangle$ and $\langle s^2\rangle^{1/2}$ from the *Polymer Handbook*,[11] we obtain $\gamma_{cr} = 1700\, c(M\times 10^{-6})^{-1.30}$ s^{-1} for HPAM 0%.

$$\gamma_{cr} = 4000\, c(M\times 10^{-6})^{-1.23}\ s^{-1} \quad \text{for PS–T}$$

and

$$\gamma_{cr} = 8000\, c(M\times 10^{-6})^{-1.00}\ s^{-1} \quad \text{for PS–C.}$$

The only experimental results which show a decrease in adsorbed thickness with shear rate of the type proposed are those of Lee and Fuller.[4] Their critical shear rate ($\sim 10^4$) would correspond to our formula for a tail segment with $M = 10^6$, or a loop with $M = 5\times 10^6$, so that a molecule with $M = 20\times 10^6$ should be attached at about five points. The discussion in the previous section predicts only one or two points of attachment, because of the large adsorbed thickness. However, the agreement is reasonable considering the crudeness of the model.

Cohen and Metzner[3] also obtain a decrease in L_H with increasing γ. Their critical shear rate would correspond to a tail with $M = 16\times 10^6$, an order of magnitude larger than the molecules they use. This result is what might be expected if their layer consists of a loosely linked network of molecules most of which are not attached directly to the surface.

Silberberg[1] and Gramain and Myard[2] obtain an increase of L_H with shear rate. In the case of Gramain and Myard, L_H increases to three to nine times its small-shear-rate value. The critical shear rates γ_{cr} at which this increase occurs are somewhat less than that at which our model predicts a decrease in L_H, taking into account the number of points of attachment predicted from $L_H(0)$ in Sec. V A. Thus, the increase apparently occurs before the molecules are fully extended.

Two possible mechanisms might be responsible for this increase in L_H with γ. In Gramain and Myard's experiments (but not in Silberberg's), the pore radii $\bar{r}$ are of the same order as the extended length of the molecules, which might allow localized blockages of the pores by a sort of "logjam" effect. One might expect more suitable sites for such pileups to occur in the Milipore and Sartorius filters which have "a spongy structure" rather than in the "nice cylindrical pores" of the Nuclepore filters, so accounting for the higher γ_{cr} in the latter case. Gramin and Myard present evidence that γ_{cr} depends more on $\bar{r}$ than on molecular weight, which might also be considered to support this hypothesis. The instantaneous return of L_H to its low-shear value as γ is reduced, as observed, could be due to Brownian forces breaking up the jams as soon as the pressure on them is released. Unfortunately, the single-segment model dealt with here cannot be used to investigate even the possibility of occurrence of such blockages, let alone their quantitative properties.

The other possible mechanism, which was suggested by Gramain and Myard,[2] involves elongational components in the flow. These might arise in two ways. Firstly, if the diameter of the "tubes" through which the solution is passed does not remain constant, the flow will contain an elongational component. This is probably not true in Silberberg's experiment, which used glass capillaries with surface roughness an order of magnitude smaller than L_H, nor in the Nuclepore filters used by Gramain and Myard. The spongy structure of the Millipore and Satorious filters used by these authors, however, would lead to a complex flow regime. Secondly, the segments protruding from the surface are quite closely packed, so that the flow must weave between them. Both

This article is copyrighted as indicated in the article. Reuse of AIP content is subject to the terms at: http://scitation.aip.org/termsconditions. Downloaded to IP: 149.106.210.114 On: Sun, 23 Nov 2014 18:03:34

effects must lead to deviations from the simple shear flow which we have assumed. In the first case, the elongational component of the flow will be constant with time, but will vary from segment to segment. In the second, it may fluctuate over times of order τ_1, the time in which a segment's configuration can change significantly. The possibility of elongational effects such as those explaining the increase in L_H was mentioned by Gramain and Myard.[2]

C. Elongational flow effects

To obtain a rough idea of the magnitude of these effects, consider a single-bead tail segment with Warner spring (so $\tau_1 = K_0/\beta$) in a flow which contains a small constant elongational component as well as a simple shear component. That is, let $\mathbf{v} = \mathbf{L}\mathbf{r}$, where

$$\mathbf{L} = \gamma \begin{bmatrix} \epsilon_1 & 1 & 0 \\ 0 & \epsilon_2 & 0 \\ 0 & 0 & -\epsilon_1 - \epsilon_2 \end{bmatrix}. \tag{5.1}$$

Here, ϵ_1 and ϵ_2 are assumed constant with time, but can take either positive and negative values, remaining fairly small compared to unity. It is to be expected that as the flow rate increases, its elongational component should increase more or less proportionately, so that the values taken by ϵ_1 and ϵ_2 remain the same as γ increases. This flow does not satisfy the zero-slip condition on the wall at $y = 0$; however, if a boundary layer of thickness δ is added to account for this (by superimposing a stagnation flow on a simple shear flow), simulation shows that $\langle y_1 \rangle$ varies by only a few percent even for δ of the same order as $\langle y_1 \rangle$.

The friction forces in the y direction, due to the elongational component of the flow, become significant when $\gamma\epsilon_2\tau_1 \sim 1$, so that the critical shear rate at which $\langle y_1 \rangle$ first becomes affected is

$$\gamma_{cr} = (\epsilon_2\tau_1)^{-1}. \tag{5.2}$$

In the limit of large γ the molecule would be fully extended along the streamline $y = (\epsilon_2 - \epsilon_1)x$, so

$$\langle y_1 \rangle = (\epsilon_2 - \epsilon_1)R\,[1 - (\epsilon_2 - \epsilon_1)^2]^{-1/2},$$

provided $\epsilon_2 > \epsilon_1$; otherwise $\langle y_1 \rangle \to 0$ as $\gamma \to \infty$. See Fig. 7 for some typical simulation results (with $\epsilon_1 = -\epsilon_2$). Assuming that ϵ_1 and ϵ_2 are equally likely to take positive and negative values, and that ϵ_1 and ϵ_2 take values of similar magnitude $\bar{y}(\gamma)$ the ensemble average of $\langle y_1 \rangle$, will tend to a value of order $\frac{1}{2}\epsilon_2 R$ as $\gamma \to \infty$. That is

$$\frac{L_H(\infty)}{L_H(0)} = \frac{\bar{y}(\infty)}{\bar{y}(0)} \simeq \left(\frac{\pi}{8}\right)^{1/2} \epsilon_2 b. \tag{5.3}$$

The most complete results obtained by Gramain and Myard[2] are those for HPAM 0% passed through Millipore (MS) and Sartorius (SM) filters. Here,

$$L_H(0)/\langle s^2 \rangle^{1/2} = 2\text{–}2.5,$$

which, when compared with the theoretical result $\langle y_N \rangle / \langle s^2 \rangle^{1/2} = 2.5$ (Fig. 2), suggests that the molecules are sufficiently densely packed to give $L_H \sim \langle y_N \rangle$. The largest likely value of R for a segment is about $\frac{1}{2} R_M$ (corresponding to a molecule attached only at both ends—a single loop—or at its center—two tails), but $R_M/L_H(\infty) = 6$, so

$$\bar{y}(\infty) \simeq \tfrac{1}{2}\epsilon_2 R \lesssim \tfrac{1}{4}\epsilon_2 R_M \simeq \tfrac{3}{2}\epsilon_2 L_H(\infty) \tag{5.4}$$

which is possible only if $\epsilon_2 \gtrsim \frac{2}{3}$. This is rather large, even for the irregularly shaped pores of these filters. For PS in these filters, the values of $R_M/L_H(\infty)$ seem to be somewhat larger, which may correspond to more attachment points per molecule or less dense packing. For HPAM in Nuclepore filters, the above analysis gives $\epsilon_2 \gtrsim 4/69 = 0.06$. It makes sense that ϵ_2 should be less in these cylindrical pores. However, $L_H(\infty)/L_H(0)$ is similar for the two types of filters, which suggests that ϵ_2 is also similar [Eq. (5.3)].

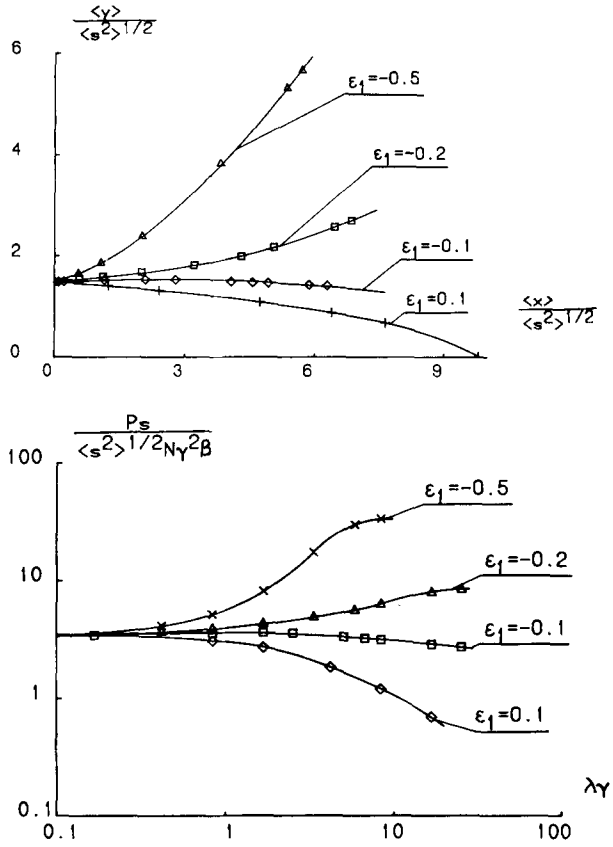

FIG. 7. (a) Elongational flow effects on the mean configuration of a one bead Rouse model with the Warner spring ($b = 5$) [$(\langle y \rangle/\langle s^2 \rangle^{1/2})$ vs $(\langle x \rangle/\langle s^2 \rangle^{1/2})$]. (b) Elongational flow effects on the power dissipation of a one bead Rouse model with the Warner spring ($b = 5$) [$(P_s/\langle s^2 \rangle N\gamma^2\beta)$ vs $\lambda\gamma$].

As suggested in Sec. V A, we will henceforth assume that a molecule is typically attached at only one or two points, at least for HPAM. Using $\epsilon_2 = \frac{2}{3}$ and the experimental values of γ_{cr} gives, from Eq. (5.3), $\tau_1 = 0.003$–0.005 s for HPAM 0% in a Nuclepore filter. These values are only weakly dependent on M_w. For a bead-spring segment of molecular weight M, however, theory gives $\tau_1 = 4[\eta]_0 \eta_s M/RT$, where $[\eta]_0 = 0.006\,31\, M^{0.8}$ ml/g.[11] If $M = \frac{1}{2} M_w$, this gives τ_1 varying from 0.003 to 1 s as M_w varies from 320 000 to 8 200 000. For τ_1 to remain constant, the number of segments would have to increase linearly with M_w. In this case L_H would also be independent of M_w, in contradiction to the experimental results.

We conclude from the above discussion that while the introduction of an elongational component to the flow does

This article is copyrighted as indicated in the article. Reuse of AIP content is subject to the terms at: http://scitation.aip.org/termsconditions. Downloaded to IP: 149.106.210.114 On: Sun, 23 Nov 2014 18:03:34

lead to an increase in L_H with γ, the increase predicted is not as large as that found experimentally and the critical shear rate at which it occurs does not correspond well. Thus, the other possible explanation, pore blockages (for which, however, our model is inadequate) seems more likely.

VI. CONCLUSIONS

We have shown that the bead-spring model for a molecular segment with finite-extension springs predicts quite well some of the experimental results obtained for flow past an adsorbed polymer layer,[4] but not others.[1–3] Possible refinements model for a single segment include displacement-dependent friction coefficients,[12,13] internal damping,[14] nonfreely rotating beads,[13] or hydrodynamic interaction[5] are not expected to change the qualitative behavior of L_H as γ varies. This assertion is supported by a few simulations we have run incorporating bead-to-bead and bead-to-wall hydrodynamic interaction, and nonfreely rotating beads. [The latter case involves replacing the velocity gradient tensor $\mathbf{L}$ by an effective velocity gradient tensor $\mathbf{L}-\epsilon(\mathbf{L}+\mathbf{L}^T)$, where ϵ is some function of the distance between the beads.[13]]

A logjam effect leading to pore blockage is suggested as a possible explanation of the increase in L_H with γ in Ref. 2. It may be possible to simulate this effect using a cluster of adjacent segments with interaction between them.

ACKNOWLEDGMENTS

It is a pleasure to acknowledge the support of the Australian Research Grants Scheme (A.R.G.S.). We thank Dr. John Hinch of Cambridge University for his comments on an earlier version of this paper and the anonymous referee for acquainting us with the important experimental results in Refs. 3 and 4.

APPENDIX: DERIVATION OF EQS. (3.8) AND (3.9)

The joint probability density of the displacements y_i normal to the wall in the case of the Rouse model are

$$P^T(\mathbf{y}) = C_N^T \exp\{-\tfrac{1}{2}[\,y_1^2 + (y_2-y_1)^2 + \cdots + (y_N - y_{N-1})^2]\} \tag{A1}$$

for a tail, and

$$P^L(y) = C_N^L \exp\{-\tfrac{1}{2}[\,y_1^2 + (y_2-y_1)^2 + \cdots + (y_N - y_{N-1})^2 + y_N^2]\} \tag{A2}$$

for a loop. In order to find the normalizing constants C_N, it is necessary to integrate the exponentials over the accessible region $y_i > 0$.

For the tail case, the transformation

$$\eta_1 = y_1 \quad \text{and} \quad \eta_i = y_i - y_{i-1} \quad \text{for } i = 2,\ldots,N. \tag{A3}$$

gives

$$(C_N^T)^{-1} = \int\cdots\int \exp\left(-\frac{1}{2}\sum_{i=1}^{N}\eta_i^2\right) d\eta_1\cdots d\eta_N \,. \tag{A4}$$

For the loop, the transformation differs according as the number of beads is odd ($N = 2M-1$) or even ($N = 2M$). In both cases,

$$\eta_i = \left(\frac{i+1}{i}\right)^{1/2} y_i - \left(\frac{i}{i+1}\right)^{1/2} y_{i+1}\,, \tag{A5}$$

$$\eta_{N-i+1} = \left(\frac{i+1}{i}\right)^{1/2} y_{N-i+1} - \left(\frac{i}{i+1}\right)^{1/2} y_{N-i}$$

for $i = 1,2,\ldots,M-1$. In the odd case,

$$\eta_M = \left(\frac{2}{M}\right)^{1/2} y_M \,. \tag{A6}$$

In the even case,

$$\eta_M = \frac{N+1}{N}(y_M + y_{M+1}),$$

$$\eta_{M+1} = \frac{1}{N}(y_M - y_{M+1})\,. \tag{A7}$$

In both cases

$$(C_N^L)^{-1} = (N+1)^{-1/2}\int\cdots\int \exp\left(-\frac{1}{2}\sum_{i=1}^{N}\eta_i^2\right) \times d\eta_1\cdots d\eta_N \,. \tag{A8}$$

For $N = 1$ and 2, these integrals are straightforward to evaluate. For $N = 3$, we proceed as follows.

1. Tail case

Define polar coordinates by

$$\eta_1 = r\cos\theta, \quad \eta_2 = r\sin\theta\cos\phi, \quad \eta_3 = r\sin\theta\sin\phi \tag{A9}$$

so that

$$(C_3^T)^{-1} = \left(\frac{\pi}{2}\right)^{1/2}\int\int \sin\theta\, d\theta\, d\phi \,. \tag{A10}$$

Noting that $\sin\theta > 0$ in the range $(0,\pi)$, the region of integration $\eta_1 > 0$, $\eta_2 + \eta_2 > 0$, $\eta_1 + \eta_2 + \eta_3 > 0$ becomes

$$\cot\theta > \max(0, -\cos\phi, -(\cos\phi + \sin\phi)) \tag{A11}$$

so that

$$(C_3^T)^{-1} = \left(\frac{\pi}{2}\right)^{1/2}\left\{2\pi - \int_{-\pi}^{-\pi/4} d\phi \int_{\cot^{-1}[-\sqrt{2}\cos(\phi-\pi/4)]}^{\pi/2} \times \sin\theta\, d\theta - \int_{\pi/2}^{\pi} d\phi \int_{\cot^{-1}(-\cos\phi)}^{\pi/2} \sin\theta\, d\theta\right\}. \tag{A12}$$

Carrying out the first integration and using the identity

$$\cos(\cot^{-1} z) = z(1+z^2)^{-1/2}$$

gives

$$(C_3^T)^{-1} = \left(\frac{\pi}{2}\right)^{1/2}\left\{2\pi + \int_{-\pi}^{-\pi/4} \sqrt{2}\cos\left(\phi - \frac{\pi}{4}\right) \times\left[1 + 2\cos\left(\phi - \frac{\pi}{4}\right)\right]^{-1/2} d\phi + \int_{\pi/2}^{\pi} \cos\phi\,(1+\cos^2\phi)^{-1/2} d\phi\right\}. \tag{A13}$$

These integrals can be carried out by standard means, leading to

$$(C_3^T)^{-1} = \frac{5}{4}\left(\frac{\pi}{2}\right)^{3/2}. \tag{A14}$$

This article is copyrighted as indicated in the article. Reuse of AIP content is subject to the terms at: http://scitation.aip.org/termsconditions. Downloaded to IP: 149.106.210.114 On: Sun, 23 Nov 2014 18:03:34

2. Loop case

Defining polar coordinates

$$\eta_2 = r\cos\theta, \quad \eta_3 = r\sin\theta\cos\phi, \quad \eta_1 = r\sin\theta\sin\phi \tag{A15}$$

transforms the region of integration $\eta_2 > 0$, $\sqrt{2}\,\eta_1 + \eta_2 > 0$, $\sqrt{2}\,\eta_3 + \eta_2 > 0$ to

$$\cot\theta > \max(0, -\sqrt{2}\cos\phi, -\sqrt{2}\sin\phi)\,. \tag{A16}$$

The integration then proceeds as before, leading to

$$(C_3^L)^{-1} = \left(\frac{\pi}{2}\right)^{3/2}. \tag{A17}$$

[1] A. Silberberg, Colloq. Int. C.N.R.S. **233**, 81 (1974).
[2] Ph. Gramain and Ph. Myard, Macromolecules **14**, 180 (1981).
[3] Y. Cohen and A. B. Metzner, Macromolecules **15**, 1425 (1982).
[4] J. J. Lee and G. G. Fuller, Macromolecules (in press).
[5] R. B. Bird, O. Hassager, R. C. Armstrong, and C. F. Curtiss, *Kinetic Theory*, (Wiley, New York, 1977), Vol. 2, Chap. 12.
[6] E. A. Dimarzio and R. J. Rubin, J. Polym. Sci. **16**, 457 (1978).
[7] G. G. Fuller, J. Polymer Sci. Polym. Phys. Ed. **21**, 151 (1983).
[8] H. R. Warner, Jr., I. EC Fundam. **11**, 379 (1972).
[9] D. L. Ermak and H. Buckholz, J. Comput. Phys. **35**, 167 (1980).
[10] P. G. Reinhall, Dynamics Laboratory Report DYNL-82-2, California Institute of Technology (1982).
[11] *Polymer Handbook*, 2nd ed., edited by J. Brandrup and E. H. Immergut (Wiley, New York, 1975), Part IV-9.
[12] R. I. Tanner, Trans. Soc. Rheol. **19**, 557 (1975).
[13] E. J. Hinch, Colloq. Int. C.N.R.S. **233**, 241 (1974).
[14] N. Phan-Thien, J. D. Atkinson, and R. I. Tanner, J. Non-Newt. Fluid Mech. **3**, 309 (1978).

This article is copyrighted as indicated in the article. Reuse of AIP content is subject to the terms at: http://scitation.aip.org/termsconditions. Downloaded to IP: 149.106.210.114 On: Sun, 23 Nov 2014 18:03:34